Optical dipole traps and atomic waveguides based on Bessel light beams

Jochen Arlt and Kishan Dholakia

School of Physics and Astronomy, University of St. Andrews, North Haugh, St. Andrews, Fife KY16 9SS Scotland, United Kingdom

Josh Soneson and Ewan M. Wright

Optical Sciences Center and Program for Applied Mathematics, University of Arizona, Tucson, Arizona 85721

We theoretically investigate the use of Bessel light beams generated using axicons for creating optical dipole traps for cold atoms and atomic waveguiding. Zeroth-order Bessel beams can be used to produce highly elongated dipole traps, allowing for the study of one-dimensional trapped gases and realization of a Tonks gas of impenetrable bosons. First-order Bessel beams are shown to be able to produce tight confined atomic waveguides over centimeter distances.

I. INTRODUCTION

The experimental realization of Bose-Einstein condensation (BEC) in dilute alkali vapors [1,2] has generated substantial theoretical and experimental research activity [3]. BEC provides an important quantum system where one can observe various phenomena such as superfluidity [4], vortices [5,6], spin domains [7], or solitonlike behavior [8–10]. Central to future advances with these quantum-degenerate systems is their manipulation by external potentials. The use of light fields offers an exciting avenue in this respect, as optical potentials can be state independent, can offer an array of spatial forms, and can be rapidly switched. They offer very good prospects for dipole traps and matter-wave guides.

Previous work has been reported for optical dipole traps based on standard Gaussian light beams [11–13]. Free-space propagating light beams such as Laguerre-Gaussian light beams [14] and Bessel light beams [15] are excellent candidates for advanced all-optical manipulation of quantum gases. Laguerre-Gaussian light beams offer a dark hollow central region for guiding and focusing atoms [16,17]. Their annular form can also be used to realize toroidal optical dipole traps for BEC [18], enabling studies of persistent currents. Bessel light beams are solutions of the scalar Helmholtz equation that are propagation invariant. This immunity to diffraction, coupled with the small size of their central region, means they offer unique characteristics in the optical domain. In this work we discuss the use of Bessel light beams for trapping and guiding cold atoms at or close to quantum degeneracy. Specifically we study the Bessel light beam optical dipole trap, with the aim of generating one-dimensional quantum gases. In particular we look at a possible realization of a Tonks gas of impenetrable bosons which exhibit fermioniclike excitations [19]. Furthermore, we analyze in detail the waveguiding of a matter-wave beam along a higher-order Bessel light beam. This method could provide an important route to realizing all-optical atom interferometers and furthering the loading of magnetic waveguides.

II. BESSEL LIGHT BEAMS

In this section we review the basics of the generation of Bessel light beams. Ideal forms of such beams are impossible to realize, as they would have an infinite extent and carry infinite power [15]. However, finite approximations of these beams can be realized that propagate over extended distances in a diffraction-free manner. Holographic methods offer an efficient generation of Bessel beams [20,21]. Another very efficient method to generate an approximation to a Bessel beam is by use of a conically shaped element termed an ''axicon,'' and it is this form of Bessel beam generation that we concentrate upon in this work. This generation method was discussed in detail elsewhere [22,23], but we review it here for completeness and clarity in notation. Our main interest is using zeroth-order Bessel beams for optical dipole traps and first-order Bessel beams for atomic waveguiding, and we shall concentrate on these cases.

Bessel beams are solutions of the free-space wave equation which propagate with an unchanging beam profile along the propagation axis which we take as z in cylindrical coordinates (r,θ,z). The electric field of a monochromatic, linearly polarized ideal Bessel beam of order l and frequency ω_L is [15,20–22]

$$\mathbf{E}(r,\theta,z,t) = \frac{\mathbf{x}}{2}[E_0 J_l(k_r r)e^{i(k_z z + l\theta - \omega_L t)} + \text{c.c.}], \quad (1)$$

where E_0 is a scale electric-field value; J_l is the lth order Bessel function; $l>0$ is the azimuthal mode number, which we take as positive for simplicity in notation; and k_r and k_z are the radial and longitudinal wave vectors such that $k^2 = k_r^2 + k_z^2$, with $k = \omega_L/c = 2\pi/\lambda_L$. The zeroth-order solution J_0 has a central maximum surrounded by concentric rings of roughly equal power, while the higher-order solutions J_l have a zero on-axis intensity with concentric rings.

The method of generating a Bessel beam by use of an axicon is based on the observation that the Fourier transform of the Bessel beam solution [Eq. (1)] over the transverse plane (r,θ) is an infinitely high ring in the spatial frequency domain peaked at $K = k_r$, where the phase varies from zero to $2\pi l$ around the peak: the Bessel beams may therefore be viewed as a superposition of plane waves with transverse wave vectors lying on a ring of magnitude k_r. A finite realization of such a beam may be produced by passing a Laguerre-Gaussian (LG) beam of order l through an axicon,
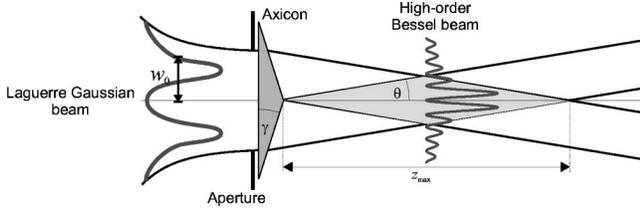
FIG. 1. Illuminating an axicon with a LG mode of order l produces a Bessel beam of the same order within the shaded region.

as illustrated in Fig. 1. The axicon is a conically shaped optical element which imparts a phase shift $\phi_{ax}(r,\theta)=k_{ax}r$ to an incident field where $k_{ax}=k(n-1)\gamma$, n being the refractive index of the axicon material, and γ the internal angle of the element. By choosing $k_{ax}=k_r$ for a specific Bessel beam, the axicon imposes a ring of transverse wave vectors characteristic of the Bessel beams on the incident beam, and these plane waves come together past the axicon to produce a Bessel beam. Single-ringed LG beams (i.e., with a radial mode index $p=0$), which may be produced using holographic elements, have electric-field envelopes (plane-wave factor $\exp[i(kz-\omega_L t)]$ removed) at a focus of the form [14]

$$\mathcal{E}_l(r,\theta,z=0)=\sqrt{\frac{2P_0}{\pi w_0^2 l!}}\left(\frac{2r^2}{w_0^2}\right)^{l/2}\exp(-r^2/w_0^2)e^{il\theta},$$
(2)

where P_0 is the power at $z=0$ incident on the axicon, w_0 is the Gaussian spot size, and l is the azimuthal mode number. Then a LG mode of order l incident on an axicon with $k_{ax}=k_r$ has the appropriate azimuthal phase variation to produce an lth-order Bessel beam past the axicon. In particular, from geometrical considerations and for a LG mode of size w_0, we expect the ring of plane waves imposed by the axicon to overlap spatially over a longitudinal range $z_{max}\sin(\vartheta)\approx w_0$, with $\sin(\vartheta)=k_r/k$. This gives the estimate [23]

$$z_{max}=\frac{kw_0}{k_r}$$
(3)

for the range over which the plane waves overlap, and produce a finite realization of the Bessel beam profile $J_l(k_r r)$ past the axicon: The larger the input spot size w_0, the larger the center portion of the transverse plane over which the actual field approaches the ideal Bessel beam.

Numerical simulations and accompanying experiments have verified this physical picture for Bessel beam generation using an axicon [22,23]. The numerical simulations used the Fresnel diffraction integral to propagate the input LG field [Eq. (2)] times the phase aberration $\exp[i\phi_{ax}(r,\theta)]$ due to the axicon, to distances beyond the axicon. Figure 2 shows a gray-scale plot of the field intensity $I(x,y=0,z)$ as an example of this numerical propagation for $l=1$, $w_0=0.29$ mm, $\lambda_L=780$ nm, $n=1.5$, and $\gamma=1°$, giving $k_r=6.8\times10^4$ m^{-1}. For this example $z_{max}=3.4$ cm, and the simulation shows that this indeed estimates the scale of the

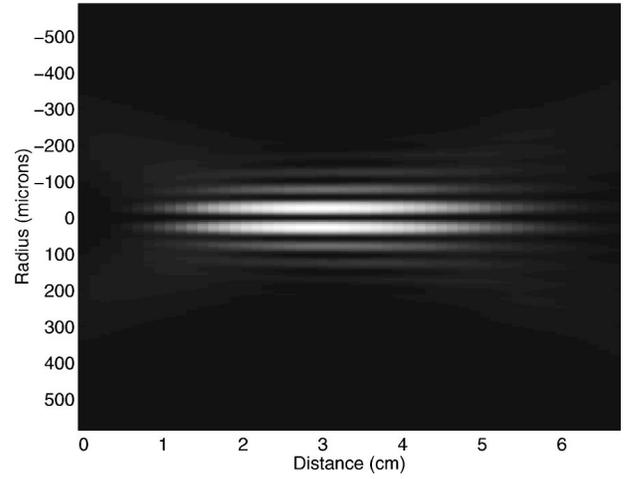

FIG. 2. Gray-scale plot of the intensity $I(x,y=0,z)$ for an input LG beam with $l=1$ showing Bessel beam formation over an elongated distance. Other parameters are $w_0=290$ μm, $\lambda_L=780$ nm, $n=1.5$, and $\gamma=1°$, giving $z_{max}=3.4$ cm and $z_{peak}=2.95$ cm.

Bessel beam propagation. As expected for a J_1 beam the intensity profile has a dark fringe at the center of width of about $w_B=1/k_r=14.7$ μm.

The evolution of the field past the axicon may also be approximated using the method of a stationary phase applied to the Fresnel integral [23], which yields the following expression for the field intensity $I_l(r,z)$ for an lth-order LG input mode:

$$I_l(r,z)\approx\frac{\pi 2^{l+1}}{l!}(k_r w_0)\left(\frac{P_0}{\pi w_0^2/2}\right)\left(\frac{z}{z_{max}}\right)^{2l+1}$$
$$\times\exp(-2z^2/z_{max}^2)J_l^2(k_r r),$$
(4)

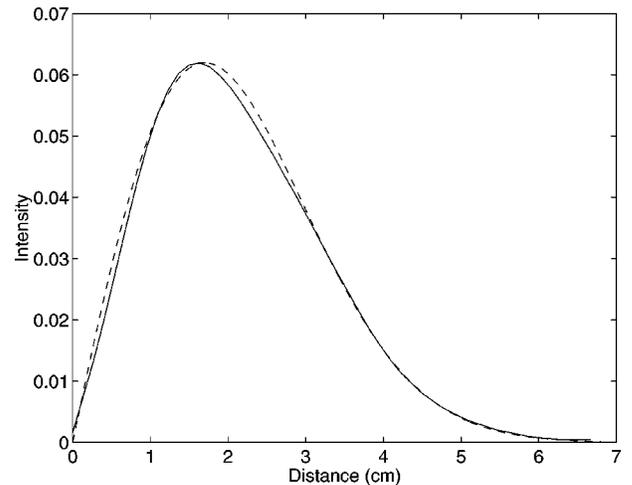with z_{max} given by Eq. (3). Figure 3 shows the on-axis in-

FIG. 3. On-axis intensity variation for an input $l=0$ LG beam using both the exact Fresnel integral approach (solid line) and expression (4) based on the stationary phase approximation (dashed line). All other parameters are the same as in Fig. 2.

tensity $I(0,z)$ versus the propagation distance z past the axicon obtained using both the Fresnel integral approach (solid line) and the approximate solution [Eq. (4)] (dashed line) for the same parameters as Fig. 2, except $l=0$, with excellent agreement (for $l=0$ the intensity has a peak on-axis). In particular, by differentiating Eq. (4), we find that the peak intensity evaluated over the whole transverse plane occurs at

$$z_{peak} = \frac{\sqrt{2l+1}}{2} z_{max}, \quad (5)$$

which gives $z_{peak} = 1.7$ cm, in excellent agreement with the results in Fig. 3. The approximate expression [Eq. (4)] is applicable over the center region of the Bessel beam if $z > k/k_r^2$ [23]. Using Eq. (3), this condition can be written as $z > z_{max}^2/(kw_0^2)$: Recognizing that $kw_0^2 = 2z_R$ is twice the Rayleigh range z_R of the input LG beam [14], and $w_B = 1/k_r$ is a measure of the width of the central lobe of the J_0 Bessel beam or the central dark fringe for a J_1 beam, we see that, if

$$\frac{z_{max}}{z_R} = \frac{2w_B}{w_0} \ll 1, \quad (6)$$

then Eq. (4) should be valid over most of the propagation range of the Bessel beam around the position of the peak z_{peak}. That is, under conditions where the central spot or dark fringe of the Bessel beam is narrow compared to the input LG spot size, which is what we want, the stationary phase approximation should be valid. For the above examples, $w_B/w_0 = 1/19.7$, and this is typical of parameters we consider. We shall assume that this condition is satisfied hereafter, and use the approximate expression [Eq. (4)] in the remainder of this paper.

Finally, we point out one further feature of Bessel beams that highlights their utility, namely, that their radial width $w_B = 1/k_r = 1/[k(n-1)\gamma]$ is determined solely by the laser wavelength and the axicon parameters, whereas their longitudinal extent $z_{max} = kw_0/k_r = kw_0 w_B$ is also dependent on the incident LG spot size w_0. This means that the longitudinal extent and radial confinement can be varied independently. This is in contrast to a Gaussian beam of equal spot w_0, for which the longitudinal extent of the focus is the Rayleigh range $z_R = kw_0^2/2$.

III. BESSEL OPTICAL DIPOLE TRAPS

In this section we examine the use of zeroth-order or J_0 Bessel beams for creating elongated optical dipole traps for Bose-Einstein condensates, and assess their utility for realizing one-dimensional trapped gases and a Tonks gas [19] of impenetrable bosons [24,25]. Here we concentrate on the case of bosonic atoms, but similar considerations apply to degenerate fermionic atoms [26] in Bessel beam traps.

A. Gross-Pitaevskii equation

The Gross-Pitaevskii equation (GPE) describing the macroscopic wave function $\psi(\mathbf{r},t)$ of an N-atom Bose-Einstein condensate in an optical dipole trap can be written as [27]

$$i\hbar \frac{\partial \psi}{\partial t} = -\frac{\hbar^2}{2M} \nabla^2 \psi + V(r,z)\psi + U_0 N |\psi|^2 \psi, \quad (7)$$

where $\nabla^2 = \nabla_r^2 + \partial^2/\partial z^2$ is a Laplacian, which is the sum of the radial and longitudinal Laplacians; M is the atomic mass; and $U_0 = 4\pi\hbar^2 a/M$ is the effective three-dimensional short-range interaction strength, with a being the s-wave scattering length. The potential term on the right-hand side,

$$V(r,z) = \frac{\hbar\Gamma^2}{8\Delta} \left(\frac{I(r,z)}{I_{Sat}} \right), \quad (8)$$

describes the optical dipole potential where $\Delta = \omega_L - \omega_A$ is the laser detuning from the optical transition frequency ω_A, Γ is the natural linewidth of the optical transition, I_{Sat} is the resonant saturation intensity, and $I(\mathbf{r},t) = \frac{1}{2}\epsilon_0 c|E(r,z)|^2$. For a red-detuned laser the potential is negative, and the atoms are attracted to the regions of high intensity, whereas for a blue-detuned laser the atoms are repelled into the low-field regions.

B. Optical dipole potential

Here we investigate the properties of an optical dipole trap formed using a red-detuned J_0 beam, so that the atoms are attracted to the intense central maximum of the intensity distribution given by Eq. (4) with $l=0$:

$$I_0(r,z) \approx 2\pi k_r w_0 \left(\frac{P_0}{\pi w_0^2/2} \right) \left(\frac{z}{z_{max}} \right) \exp(-2z^2/z_{max}^2) J_0^2(k_r r). \quad (9)$$

We are primarily interested in tight bound optical dipole traps, so we shall approximate the optical dipole potential [Eq. (8)] using the parabolic approximation to the full intensity $I_0(r,z)$ around the intensity maximum at $(r=0, z = z_{peak})$,

$$V(r,z) - V(0,z_{peak}) \approx \frac{1}{2} M\Omega_{r0}^2 [r^2 + \lambda^2 (z - z_{peak})^2], \quad (10)$$

with

$$\Omega_{r0}^2 = \exp(-1/2) \frac{\hbar\Gamma^2}{4|\Delta|} \frac{P_0}{MI_{Sat}} \frac{k}{z_{max}} k_r^2,$$

$$\lambda = \frac{2\sqrt{2}}{kw_0} = 2.83 \frac{w_B}{z_{max}}. \quad (11)$$

A red-detuned ($\Delta < 0$) J_0 optical dipole potential therefore provides confinement in both radial and longitudinal directions. Here Ω_{r0} is the radial oscillation frequency, with a corresponding ground-state oscillator width $w_{r0} = \sqrt{\hbar/M\Omega_{r0}}$, and λ is the ratio between the longitudinal and radial trap frequencies $\Omega_{z0}/\Omega_{r0} = \lambda$ [28–30], which also de-

termines the aspect ratio between the radial and longitudinal ground-state widths $w_{r0}/w_{z0} = \sqrt{\lambda}$ (in the absence of many-body repulsion). We remark that even for tight transverse confinement, anharmonic corrections beyond the parabolic approximation for the longitudinal (z) variation of the optical dipole potential [Eq. (10)] are generally required. This is evident from Fig. 3, where the on-axis intensity variation for the J_0 Bessel beam is not symmetric around the peak. For this work we shall restrict ourselves to the parabolic approximation. However, we remark that anharmonic corrections to the parabolic approximation can have pronounced effects on trap properties such as the condensate fraction and the frequencies of the collective excitations that can be supported by Bessel atomic waveguides, especially for shallow traps [31].

So far we have ignored the effects of gravity, which we assume acts in the radial direction so the longitudinal axis of the trap is horizontal. For tight radial confinement, the gravity will serve simply to displace the origin of the radial motion, and this applies under conditions such that $M\Omega_{r0}^2 w_{r0}^2/2 \gg Mgw_{r0}$ with $g = 9.81$ ms^{-1}. Using $w_{r0} = \sqrt{\hbar/M\Omega_{r0}}$, this leads to the condition on the confinement of the ground state, $w_{r0} \ll \sqrt[3]{\hbar^2/(2M^2g)}$. For example, for ^{85}Rb the radial confinement has to be less than 0.31 μm, whereas for ^{23}Na a confinement of $w_{r0} \ll 0.74$ μm would be sufficient. We assume that this condition is satisfied, and hereafter neglect the effects of gravity.

C. One-dimensional trapped gases

From Eq. (11), a parameter λ is seen to determine the anisotropy of the J_0 optical dipole trap. It is well known that in the limit $\lambda \ll 1$ highly asymmetric cigar-shaped traps are formed which are elongated along the longitudinal direction [28–30]. Bessel beams are exceptional in this regard, as they can produce extreme asymmetries. To illustrate this, recall that w_0 is the input LG spot size *before* the axicon, for example $w_0 = 1$ mm, so that $\lambda = 4.8 \times 10^{-4}$ for $\lambda_L = 1064$ nm. We stress that one obtains such large asymmetries using Bessel beams without sacrificing the radial confinement, as the radial ($w_B = 1/k_r$) and longitudinal (z_{max}) extents of the Bessel beam are independently variable. In contrast, for a Gaussian optical dipole trap, changing the focused spot size w_0 also changes the longitudinal extension of the dipole trap set by the Rayleigh range $z_R = kw_0^2/2$ [14].

The limit $\lambda \ll 1$ corresponds to the regime of one-dimensional trapped gases [25,29,30], in which the radial variation of the macroscopic wave function is effectively frozen as the normalized ground-state mode $u_g(r)$ of the radial optical dipole potential:

$$E_g u_g = -\frac{\hbar^2}{2M}\nabla_r^2 u_g + \frac{1}{2}M\Omega_{r0}^2 r^2 u_g. \quad (12)$$

Writing the macroscopic wave function in a form reflecting the single-radial mode nature of the solution,

$$\psi(r,z,t) = u_g(r)\phi(z,t)e^{-iE_g t/\hbar}, \quad (13)$$

and combining Eqs. (7), (10), (12), and (13), we obtain the one-dimensional Gross-Pitaevskii equation for the reduced system [29,30],

$$i\hbar\frac{\partial\phi}{\partial t} = -\frac{\hbar^2}{2M}\frac{\partial^2\phi}{\partial z^2} + \frac{1}{2}M\lambda^2\Omega_{r0}^2(z-z_{peak})^2\phi + gN|\phi|^2\phi, \quad (14)$$

where

$$g = U_0\int 2\pi r dr|u_g(r)|^4 = \frac{2\hbar^2 a}{Mw_{r0}^2} = 2\hbar\Omega_{r0}a \quad (15)$$

is the effective one-dimensional short-range interaction strength [25]. In the steady state we set $\phi(z,t) = \chi(z)\exp(-i\mu t/\hbar)$ in Eq. (14), with μ the chemical potential of the one-dimensional system. Then, using the Thomas-Fermi approximation [25] for high density in which the kinetic-energy term is neglected [28], Eq. (14) yields for the one-dimensional density

$$\rho(z) = |\chi(z)|^2 = \frac{\mu}{g}\left(1 - \frac{(z-z_{peak})^2}{z_m^2}\right), \quad |z-z_{peak}| \le z_m, \quad (16)$$

with

$$\mu = \left(\frac{3gN}{4}\right)^{2/3}\left(\frac{M\Omega_{r0}^2\lambda^2}{2}\right)^{1/3}, \quad z_m = \left(\frac{3Nw_{r0}^2 a}{\lambda^2}\right)^{1/3}. \quad (17)$$

This density solution has a peak one-dimensional density $\rho_{peak} = 1.5(N/L_z) \propto N^{2/3}$ with a longitudinal length $L_z = 2z_m$.

The Gross-Pitaevskii equation (14) was previously investigated as a model for a one-dimensional Bose-Einstein condensate in a number of situations, including the ground state [32] and dynamics [33] of cigar-shaped traps [34–36], dark solitons [30,9,37,38], bright solitons for negative scattering lengths [29,30,39], gap solitons in optical lattices [8], atom waveguides [40–42], and as a model Luttinger liquid [43]. Here our goal is to highlight the utility of J_0 optical dipole traps for experimental studies of one-dimensional trapped gases. To illustrate the basic scales involved in these elongated traps, we consider the case of the $\lambda_A = 780$ nm transition of Rb with $I_{Sat} = 16$ W/m^2 and $\Gamma = 2\pi \times 6.1$ MHz. A far red-detuned laser at a wavelength of $\lambda_L = 1064$ nm is used to generate a Bessel beam with a longitudinal extent $z_{max} = 10$ cm and a central spot of full-width radius 3 μm (corresponding to $w_B = 1.25$ μm, and consequently $w_0 = 13.6$ mm). If a laser power of $P_0 = 5$ W is used, this results in a trap potential of about -49μK depth with radial trap frequency $\Omega_{r0} = 2\pi \times 8.8$ kHz, a radial confinement of $w_{r0} = 82$ nm, and an aspect ratio of $\lambda = 3.5 \times 10^{-4}$. Then for $N = 10^4$ atoms and a scattering length $a = 5$ nm, for example, we find $L_z = 2z_m = 1.9$ mm, and a peak density $\rho_{peak} = 6.4 \times 10^4$ cm^{-1}. For comparison, a focused Gaussian with the same radial confinement (and trap depth) gives a trap with an aspect ratio of only 8×10^{-2}. We remark, however, that the

power required to obtain the same radial confinement for the Gaussian beam is much less, typically on the order of mW [11]. This arises because for the Bessel beam the trapped atoms only experience the intensity in the central peak of the beam, and the concentric rings surrounding the peak, though key in realizing the long extent of the Bessel optical dipole trap, do not directly affect the atomic confinement.

Bessel beam traps will suffer from the same loss mechanisms as other shallow far-off-resonance dipole traps. Apart from heating due to diffractive collisions with background gases [44], the trap lifetime will be limited by laser-noise-induced heating [45]. The expected loss rates due to intensity fluctuations and the pointing instability of the laser beam for a Bessel beam trap should be comparable to those in Gaussian beam traps with identical radial confinement and trap depth.

Finally, we note that the J_0 optical dipole trap provides a means to accelerate an atomic trapped one-dimensional gas. Consider a one-dimensional gas in the ground state of a J_0 trap peaked around $z = z_{peak} = k w_0 / 2 k_r$. If we now start to slowly increase the LG spot size $w_0(t)$, then the longitudinal position of the peak density of the trapped gas should vary in time according to $z_{peak}(t) = k w_0(t) / 2 k_r$. Such a scheme provides a means to impart a longitudinal velocity to an initially stationary trapped gas.

D. Realization of a Tonks gas

In the above discussion we tacitly assumed that the system of cold atoms formed a Bose-Einstein condensate. However, Petrov *et al.* [25] theoretically studied the diagram of state for a one-dimensional gas of trapped bosons, assuming $\lambda \ll 1$, and found that a true Bose-Einstein condensate, or at least a quasicondensate, with concomitant macroscopic occupation of a single state, is only attained for high enough particle numbers $N > N_*$ with

$$N_* = \left(\frac{M g w_{z0}}{\hbar^2} \right)^2 = \left[2 \left(\frac{a}{w_{r0}} \right) \left(\frac{w_{z0}}{w_{r0}} \right) \right]^2. \quad (18)$$

For $N < N_*$ and temperatures $T < N \hbar \Omega_{z0}$, one obtains a Tonks gas of impenetrable bosons for which hard-core repulsion between the bosonic atoms prevents them from penetrating through each other in the one-dimensional system, and the system acquires properties reminiscent of a one-dimensional system of fermionic atoms. This remarkable property of the Tonks gas is related to a breakdown of the spin-statistics theorem in one dimension, and is reflected in the Fermi-Bose mapping for this system first elucidated by Girardeau [46], and applied to atomic waveguides by Olshanii [24]. Recent theoretical investigations of Tonks gases showed that they can support dark soliton structures [47,48], and also that their coherence properties are significantly different from the corresponding Bose-Einstein condensate [49,50]. Furthermore, recent experimental developments suggested that Tonks gases should be realizable in magnetic atom waveguides [40–42], and Bongs *et al.* [36] proposed a hybrid trap composed of an optical dipole trap formed with a first-order LG beam combined with magnetic longitudinal

trapping. Here we examine the utility of J_0 optical dipole traps for realizing a Tonks gas.

The highly elongated Bessel beam discussed in Sec. II ($\lambda_L = 1064$ nm, $P_0 = 5$ W, $z_{max} = 10$ cm, $w_B = 1.25$ μm) would be an ideal candidate for the experimental realization of a Tonks gas. The low aspect ratio $\lambda = 3.5 \times 10^{-4}$ and tight radial confinement $w_{r0} = 82$ nm result in a high upper boundary N_* for the particle number of the Tonks gas. For the commonly used ^{87}Rb isotope with a scattering length $a = 5$ nm one finds $N_* = 420$. Although this is still a fairly low value it should be possible to experimentally realize a small ^{87}Rb Tonks gas. However, more promising would be the use of the ^{85}Rb isotope, where a Feshbach resonance can be used to tune the normally negative scattering length to positive values of several hundred nanometers magnitude [51]. As N_* is proportional to the square of the scattering length, even a moderate increase to $a = 50$ nm would make it possible to create a larger Tonks gas, with say $N = 2000$ atoms, which should be easily detectable.

The Bessel beam trap offers some advantages compared to alternative suggested approaches using magnetic waveguides [40–42] and a hybrid magnetic-optical trap [36]. First, it involves only a very simple *all-optical* system for which the aspect ratio of the trap may be controlled simply by varying the Gaussian spot size incident on the axicon. More specifically, being an all-optical system, it does not involve material surfaces as in magnetic waveguides, which can cause matter-wave decoherence [52,53]. Furthermore, it allows for the possibility of trapping multiple magnetic sublevels and the investigation of multicomponent Tonks gases, which would not be possible in the hyrbrid magnetic-optical trap of Bongs *et al.* [36].

IV. BESSEL BEAM ATOMIC WAVEGUIDES

Higher-order Bessel beams J_l with $l > 0$ have a zero on-axis intensity surrounded by intense concentric rings, and a blue-detuned beam can therefore trap atoms radially in the dark hollow core of the beam. In addition, since the intensity vanishes on-axis, the higher-order beams produce a negligible longitudinal confinement (see Fig. 2 for the J_1 Bessel beam) in comparison to the J_0 Bessel beam. The higher-order Bessel beams therefore present the opportunity to realize atomic waveguides with tight radial confinement over distances comparable to the propagation range z_{max} of the Bessel beams. Furthermore, the J_1 beam is special in that it provides a parabolic radial trapping potential to lowest order (see below), whereas the higher-order trapping potential vary as r^{2l} near the axis. We shall therefore concentrate on the J_1 atomic waveguide [54].

A. Atomic waveguide potential

Here we investigate the properties of an atomic waveguide formed using a blue-detuned ($\Delta > 0$) J_1 beam, so that the atoms are repelled into the zero intensity central minimum of the intensity distribution given by Eq. (4) with $l = 1$:

$$I_1(r,z) \approx 4\pi k_r w_0 \left(\frac{P_0}{\pi w_0^2/2}\right)\left(\frac{z}{z_{\max}}\right)^3 e^{-2z^2/z_{\max}^2} J_1^2(k_r r).$$

(19)

Substituting this expression into the optical dipole potential [Eq. (8)], we write the atomic waveguiding potential in the form

$$V(r,z) = \frac{1}{2}M\Omega_{r1}^2(z)\left(4\frac{J_1^2(k_r r)}{k_r^2}\right) \approx \frac{1}{2}M\Omega_{r1}^2(z)r^2,$$

(20)

where in the last form of the potential we used the approximation $J_1(x) \approx x/2$, which is applicable for tight radial confinement. Here the z-dependent radial oscillation frequency $\Omega_{r1}(z)$ is given by

$$\Omega_{r1}(z) = \Omega_{r1}(z_{\text{peak}})\left(\frac{z}{z_{\text{peak}}}\right)^{3/2}\exp[-0.75(z^2/z_{\text{peak}}^2 - 1)],$$

(21)

with $z_{\text{peak}} = \sqrt{3}z_{\max}/2$ the position of the peak intensity for the J_1 Bessel beam, and $\Omega_{r1}(z_{\text{peak}})$ is the peak radial oscillation frequency given by

$$\Omega_{r1}^2(z_{\text{peak}}) = \left(\frac{\sqrt{3}}{2}\right)^3 \exp(-3/2)\frac{\hbar\Gamma^2}{4|\Delta|}\frac{P_0}{MI_{\text{Sat}}}\frac{k}{z_{\max}}k_r^2.$$

(22)

In comparison to the radial oscillation frequency of the J_0 Bessel beam trap we find $\Omega_{r1}(z_{\text{peak}}) \approx 0.5\Omega_{r0}$.

The J_1 Bessel beam therefore defines an atomic waveguide whose radial confinement peaks at $z = z_{\text{peak}}$ and varies with the longitudinal coordinate z. If we take the effective length L of the waveguide to be the full width at half maximum of $\Omega_{r1}(z)$ versus z, then by inspection of Eq. (21) we find $L \approx z_{\max}$, as may have been anticipated physically based on the properties of the Bessel beams.

B. Gross-Pitaevskii equation

To examine the properties of a Bose-Einstein condensate propagating in a J_1 atom waveguide, we shall approximate the waveguide as invariant along the z axis over the length $L = z_{\max}$, and calculate the ground-state radial mode of this system. In general we should solve the propagation problem of the matter wave field through the varying atomic waveguide potential, and show how the atoms are funneled into the waveguide, but these shall be the subjects of a future paper.

To proceed, we consider the GPE (7) for a Bose-Einstein condensate of momentum p_z per atom moving along the z axis in a cylindrically symmetric J_1 Bessel atom waveguide which is invariant along the z axis. Then, writing the macroscopic wave function as

$$\sqrt{N}\psi(r,z,t) = \varphi(r)e^{i(p_z z - \mu t)/\hbar},$$

(23)

the GPE becomes

$$\left(\mu - \frac{p_z^2}{2M}\right)\varphi = -\frac{\hbar^2}{2M}\left(\frac{d^2}{dr^2} + \frac{1}{r}\frac{d}{dr}\right)\varphi + V_0 J_1^2(k_r r)\varphi$$
$$+ U_0|\varphi|^2\varphi,$$

(24)

where μ is the chemical potential, and $V_0 = 2M\Omega_{r1}^2(z_{\text{peak}})/k_r^2$ characterizes the strength of the J_1 waveguide. The wave function over the atomic waveguide effective length $L = z_{\max}$ is normalized to the number of particles:

$$z_{\max}\int_0^\infty 2\pi r\,dr|\varphi(r)|^2 = N.$$

(25)

To facilitate a numerical solution of the GPE, we introduce scaled variables [55]

$$\zeta = k_r r, \quad \varphi(r) = \sqrt{\frac{E_r}{|U_0|}}\varphi(\zeta),$$

(26)

in terms of which the GPE for $\varphi(\zeta)$ becomes

$$\alpha\varphi = -\left(\frac{d^2}{d\zeta^2} + \frac{1}{\zeta}\frac{d}{d\zeta}\right)\varphi + \beta J_1^2(\zeta)\varphi + c|\varphi|^2\varphi.$$

(27)

Here $E_r = \hbar^2 k_r^2/2M$ sets the energy scale, $\alpha = (\mu - p_z^2/2M)/E_r$ is the scaled energy eigenvalue, $\beta = V_0/E_r$, and $c = \pm 1$ sets the sign of the many-body interactions. The wave function $\varphi(\zeta)$ is now normalized as

$$\int_0^\infty \zeta\,d\zeta|\varphi(\zeta)|^2 = \eta N = n,$$

(28)

where the dimensionless variable $\eta = (k_r^2|U_0|/L)/(2\pi E_r) = 4|a|/L$.

Strictly speaking the J_1 atomic waveguide potential in GPE (27) does not have bound-state solutions, since any initial wave function localized in the central minimum of the J_1 potential will ultimately tunnel out over the finite potential barrier due to the first peak of the Bessel beam. However, for tight confined atoms the tunneling time can be made arbitrarily long, and here we ignore tunneling to lowest order. Figures 4 and 5 show the results of the numerical solution of GPE (27) for $\beta = 10^3$ and $c = 1$, that is repulsive many-body interactions. These numbers would describe, for example, a guide for rubidium with a radius of 5 μm (corresponding to $w_B = 2.78$ μm) and a length $L = 5$ cm using 40 mW of light at $\lambda_L = 1064$ nm. The numerical method used to solve Eq. (27) was the same as that in Ref. [55]. Figure 4 shows the variation of the scaled energy eigenvalue α versus the scaled number of particles $n = \eta N$; we see that as n increases, so does the energy due to the repulsive many-body interactions. For $n \to 0$ the scaled energy reduces to that of the atomic waveguide potential (see below). Figure 5 shows the scaled wave function $\varphi(\zeta)$ versus the scaled radial coordinate ζ for $n = 0.88$ ($\alpha = 50$) (solid line), $n = 13.4$ ($\alpha = 150$) (dotted line), and $n = 43$ ($\alpha = 250$) (dashed line). Here we see that as the scaled number of atoms increases, so does the width of
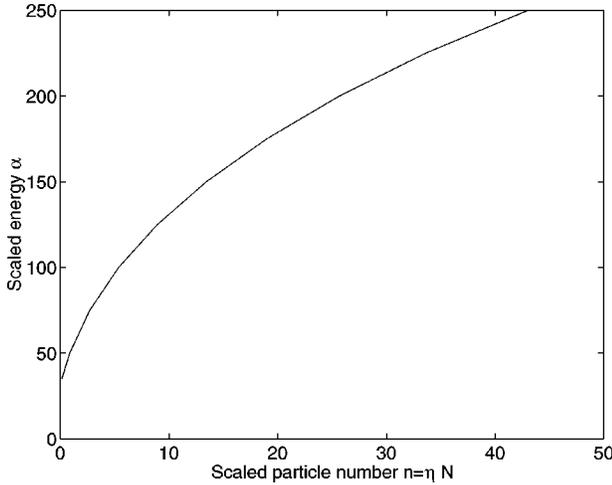
FIG. 4. Scaled energy eigenvalue α vs scaled particle number $n=\eta N$ for $\beta=10^3$. Physically, α is the chemical potential minus the longitudinal kinetic energy per particle scaled to the energy E_r, and $\beta=V_0/E_r$ measures the depth of the Bessel optical potential scaled to E_r.

the wave function, as expected physically. Clearly there is a limit to the allowable width of the wave function, and hence the number of atoms, as the tunneling out of the atomic waveguide alluded to above will become more relevant as the wave function width approaches that of the central minimum of the J_1 Bessel beam.

C. Thomas-Fermi approximation

In this section we discuss approximate solutions to GPE (27) to provide a framework for the numerical solutions. First for tight confinement, so that tunneling out of the trap is negligible, we approximate $J_1(\zeta)\approx\zeta/2$, giving

$$\alpha\varphi\approx-\left(\frac{d^2}{d\zeta^2}+\frac{1}{\zeta}\frac{d}{d\zeta}\right)\varphi+\frac{\beta\zeta^2}{4}\varphi+|\varphi|^2\varphi. \qquad (29)$$
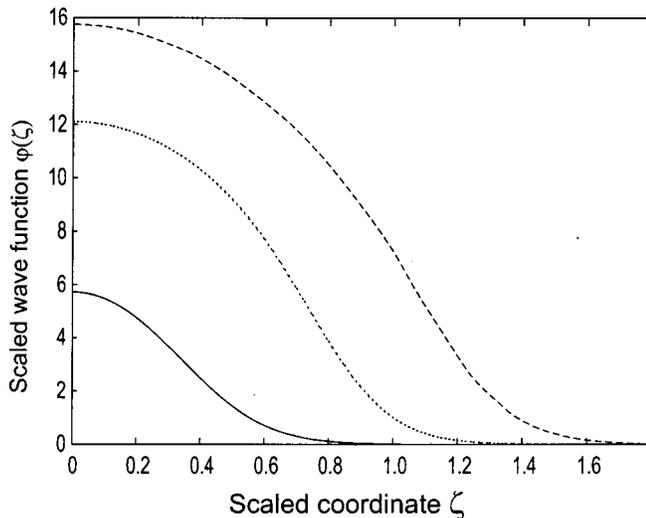

FIG. 5. Scaled transverse eigenmode $\varphi(\zeta)$ vs scaled radial coordinate ζ for $\beta=10^3$ and $n=0.88$ ($\alpha=50$) (solid line), $n=13.4$ ($\alpha=150$) (dotted line), and $n=43$ ($\alpha=250$) (dashed line).

For this to be valid the macroscopic wave function should not extend beyond the first peak of the J_1 Bessel function at $\zeta_c=1.8$. Then, in the limit of a small number of atoms $\eta N\rightarrow0$, the GPE has the Gaussian ground-state solutions

$$\varphi(\zeta)\propto\exp(-\zeta^2/\zeta_0^2), \quad \alpha=\sqrt{\beta}, \qquad (30)$$

with $\zeta_0=2\beta^{-1/4}$; this is only valid if $\zeta_0<\zeta_c$, or $\beta\gg1$. For $\beta=10^3$ this gives $\alpha=31.6$, in agreement with Fig. 4 as $\eta N\rightarrow0$. In the limit of large ηN we can use the Thomas-Fermi solution [28] in which the kinetic-energy term is neglected. This yields the solutions

$$|\varphi(\zeta)|^2=\sqrt{\eta N\beta}(1-\zeta^2/\zeta_m^2), \quad \zeta<\zeta_m=2\left(\frac{\eta N}{\beta}\right)^{1/4}, \qquad (31)$$

and $\alpha_{\mathrm{TF}}=\sqrt{\eta N\beta}$. This solution is only valid if $\zeta_m<\zeta_c=1.8$, which for a given value of β places an upper bound on the scaled number of atoms n

$$n=\eta N<\beta. \qquad (32)$$

In Figs. 4 and 5 we have restricted $n<950$, in accordance with the above upper bound, and the wave functions in Fig. 5 are all vanishingly small in the region $\zeta>\zeta_c=1.8$. As an example, for $n=43$ and $\beta=10^3$ the Thomas-Fermi solution predicts $\zeta_m=0.9$, which is smaller than the spatial extent of the wave function (dashed line) in Fig. 5, and $\alpha_{\mathrm{TF}}=207$ in comparison to $\alpha=250$ from the exact solution in Fig. 4. This discrepancy between the exact and approximate solutions is not surprising, as we used a parabolic approximation of the optical potential in the Thomas-Fermi solution. However, the Thomas-Fermi theory captures the trends of the solution.

V. SUMMARY AND CONCLUSIONS

Bessel light beams have unusual properties in the optical domain. They have an immunity to diffraction over extended distances, and offer an elongated and narrow central region. These features give them significant advantages over standard Gaussian light beams for the studies presented in this work. We have shown that zeroth-order Bessel light beams generated by the use of an axicon offer an excellent method by which to generate optical dipole traps for one-dimensional quantum gases. Typically, the ratio λ between longitudinal and transverse trap frequencies for such a trap, realized with a Bessel beam, is nearly two orders of magnitude smaller than that which can be achieved with a Gaussian beam. Furthermore, we have shown that the Bessel beam offers a potential route for an experimental realization of a Tonks gas of inpenetrable bosons. Additionally we have studied the waveguiding properties of a quantum gas along a J_1 (hollow) Bessel light beam. The nondiffracting nature and small central minimum size here make it an excellent all-optical waveguide. Such waveguiding could be used to realize the velocity filtering of cold atoms and all-optical atom interferometers, and also offer a route to load magnetic waveguides with quantum degenerate samples.

[1] M. H. Anderson, J. R. Ensher, M. R. Matthews, C. E. Wieman, and E. A. Cornell, Science **269**, 198 (1995).

[2] K. B. Davis, M. O. Mewes, M. R. Andrews, N. J. van Druten, D. S. Durfee, D. M. Kurn, and W. Ketterle, Phys. Rev. Lett. **75**, 3969 (1995).

[3] F. Dalfovo, S. Giorgini, and L. P. Pitaevskii, Rev. Mod. Phys. **71**, 463 (1999).

[4] C. Raman, R. Onofrio, J. M. Vogels, J. R. Abo-Shaeer, and W. Ketterle, e-print cond-mat/0008423.

[5] K. W. Madison, F. Chevy, W. Wohlleben, and J. Dalibard, Phys. Rev. Lett. **84**, 806 (2000).

[6] M. R. Matthews *et al.*, Phys. Rev. Lett. **83**, 2498 (1999).

[7] D. M. Stamper-Kurn *et al.*, Phys. Rev. Lett. **83**, 661 (1999).

[8] O. Zobay, S. Potting, P. Meystre, and E. M. Wright, Phys. Rev. A **59**, 643 (1999).

[9] S. Burger *et al.*, Phys. Rev. Lett. **83**, 5198 (1999).

[10] J. Denschlag *et al.*, Science **287**, 97 (2000).

[11] D. M. Stamper-Kurn, M. R. Andrews, A. P. Chikkatur, S. Inouye, H.-J. Miesner, J. Stenger, and W. Ketterle, Phys. Rev. Lett. **80**, 2027 (1998).

[12] Dallin S. Durfee, Ph. D thesis, MIT, 1999.

[13] D. Frese *et al.*, Phys. Rev. Lett. **85**, 3777 (2000).

[14] A. E. Siegman, *Lasers* (University Science Books, Sausilito, CA, 1986).

[15] J. Durnin, J. J. Miceli, and J. H. Eberly, Phys. Rev. Lett. **58**, 1499 (1987).

[16] M. Schiffer *et al.*, Appl. Phys. B: Lasers Opt. **67**, 705 (1998).

[17] J. Arlt *et al.*, Appl. Phys. B: Lasers Opt. **71**, 549 (2000).

[18] E. M. Wright *et al.*, Phys. Rev. A **63**, 013608 (2000).

[19] L. Tonks, Phys. Rev. **50**, 955 (1936).

[20] J. Turunen, A. Vasara, and A. T. Friberg, Appl. Opt. **27**, 3959 (1988).

[21] A. Vasara, J. Turunen, and A. T. Friberg, J. Opt. Soc. Am. A **6**, 1748 (1989).

[22] R. M. Herman and T. A. Wiggins, J. Opt. Soc. Am. A **8**, 932 (1991).

[23] J. Arlt and K. Dholakia, Opt. Commun. **177**, 297 (2000).

[24] M. Olshanii, Phys. Rev. Lett. **81**, 938 (1998).

[25] D. S. Petrov *et al.*, Phys. Rev. Lett. **85**, 3745 (2000).

[26] B. De Marco and D. S. Jin, Science **285**, 1703 (1999).

[27] E. M. Lifshitz and L. P. Pitaevskii, *Statistical Physics* (Pergamon Press, Oxford, 1989), Pt. 2, pp. 85–118.

[28] G. Baym and C. J. Pethick, Phys. Rev. Lett. **76**, 6 (1996).

[29] V. M. Perez-Garcia *et al.*, Phys. Rev. A **57**, 3837 (1998).

[30] Y. S. Kivshar and T. J. Alexander, e-print cond-mat/9905048.

[31] J. P. Martikainen, e-print cond-mat/0008025.

[32] L. D. Carr *et al.*, Phys. Rev. A **62**, 063610 (2000).

[33] P. Villain *et al.*, Phys. Rev. A **63**, 033607 (2000).

[34] M. R. Andrews *et al.*, Science **273**, 84 (1996).

[35] W. Ketterle *et al.*, e-print cond-mat/9904034.

[36] K. Bongs *et al.*, Phys. Rev. A **63**, 031602(R) (2001).

[37] D. L. Feder *et al.*, Phys. Rev. A **62**, 053606 (2000).

[38] L. D. Carr *et al.*, e-print cond-mat/0011397.

[39] L. D. Carr *et al.*, Phys. Rev. A **62**, 063611 (2000).

[40] J. H. Thywissen *et al.*, Eur. Phys. J. D **7**, 361 (1999).

[41] M. Key *et al.*, Phys. Rev. Lett. **84**, 1371 (2000).

[42] N. H. Dekker *et al.*, Phys. Rev. Lett. **84**, 1124 (2000).

[43] H. Monien *et al.*, Phys. Rev. A **58**, R3395 (1998).

[44] S. Bali, K. M. O'Hara, M. E. Gehm, S. R. Granade, and J. E. Thomas, Phys. Rev. A **60**, R29 (1999).

[45] T. A. Savard, K. M. O'Hara, and J. E. Thomas, Phys. Rev. A **56**, R1095 (1997).

[46] M. Girardeau, J. Math. Phys. **1**, 516 (1960); Phys. Rev. **139**, B500 (1965).

[47] M. D. Girardeau and E. M. Wright, Phys. Rev. Lett. **84**, 5691 (2000).

[48] E. B. Kolomeisky *et al.*, Phys. Rev. Lett. **85**, 1146 (2000).

[49] M. D. Girardeau and E. M. Wright, Phys. Rev. Lett. **84**, 5239 (2000).

[50] M. D. Girardeau *et al.*, Phys. Rev. A **63**, 033601 (2001).

[51] S. L. Cornish *et al.*, Phys. Rev. Lett. **85**, 1795 (2000).

[52] C. Henkel and M. Wilkens, Europhys. Lett. **47**, 414 (1999).

[53] C. Henkel, S. Poetting, and M. Wilkens, Appl. Phys. B: Lasers Opt. **69**, 379 (1999).

[54] M. Saffman, Phys. Rev. Lett. **81**, 65 (1998).

[55] S. K. Adhikari, Phys. Lett. A **265**, 91 (2000).